International Journal of Information, Control and Computer Sciences
ISSN: 2517-9942
Vol:15, No:1, 2021

# Near-Infrared Hyperspectral Imaging Spectroscopy to Detect Microplastics and Pieces of Plastic in Almond Flour

H. Apaza, L. Chévez, H. Loro

***Abstract*—**Plastic and microplastic pollution in human food chain is a big problem for human health that requires more elaborated techniques that can identify their presences in different kinds of food. Hyperspectral imaging technique is an optical technique than can detect the presence of different elements in an image and can be used to detect plastics and microplastics in a scene. To do this statistical techniques are required that need to be evaluated and compared in order to find the more efficient ones. In this work, two problems related to the presence of plastics are addressed, the first is to detect and identify pieces of plastic immersed in almond seeds, and the second problem is to detect and quantify microplastic in almond flour. To do this we make use of the analysis hyperspectral images taken in the range of 900 to 1700 nm using 4 unmixing techniques of hyperspectral imaging which are: least squares unmixing (LSU), non-negatively constrained least squares unmixing (NCLSU), fully constrained least squares unmixing (FCLSU), and scaled constrained least squares unmixing (SCLSU). NCLSU, FCLSU, SCLSU techniques manage to find the region where the plastic is found and also manage to quantify the amount of microplastic contained in the almond flour. The SCLSU technique estimated a 13.03% abundance of microplastics and 86.97% of almond flour compared to 16.66% of microplastics and 83.33% abundance of almond flour prepared for the experiment. Results show the feasibility of applying near-infrared hyperspectral image analysis for the detection of plastic contaminants in food.

***Keywords*—**Food, plastic, microplastic, NIR hyperspectral imaging, unmixing.

## I. Introduction

THE contamination of our environment by plastic and microplastic has become one of the biggest problems of this century since this material can cause serious problems to our health because it can reach us through the food chain [1]-[4]. The category of microplastic is generally defined by its size. Thus it is said that if a plastic fragment is less than 5 mm it belongs to the category of microplastic [5], [6]. In order to detect the presence of plastics and microplastics in our food, online analysis techniques are necessary to detect and quantify plastic and microplastics.

In recent years, hyperspectral image analysis (HSI) has emerged as a promising technique to assess the quality and safety of food products as it takes advantage of the integration of conventional imaging technique and spectroscopy technique, obtaining in a single spatial and spectral information system of the sample to be analyzed [7], [8], thus becoming an appropriate option in food product inspection processes.

In this work two problems are addressed, the first is to detect and quantify a piece of plastic immersed in almond seeds, and the second is to detect and quantify microplastic in almond flour. To do this, we use the technique of analyzing hyperspectral images in the near infrared in the range of 900 to 1700 nm using four hyperspectral unmixing techniques, which are LSU, NCLSU, FCLSU, and SCLSU.

## II. Materials and Methods

### A. Elements Present in the Images

Two images were studied; the first one is an image containing a piece of plastic between six almond seeds which we call image 1. This piece of plastic was taken from the top of a water bottle and will be called "plastic 1" from now on. The second image, which we call image 2, is a mixture of 10 ml of almond flour with 2 ml of pulverized plastic in a mortar to simulate the presence of microplastic, this mixture then contains 16.66% of microplastic and 83.33% of almond flour, the pulverized plastic is obtained from Petri dishes and henceforth this microplastic will be called "microplastic". Mixing was done manually with the help of a spatula. The first image consists of 135 × 118 pixels and its spectral dimension is 123 bands while the second image consists of 76 × 86 pixels, and its spectral dimension is 123 bands.

### B. NIR Hyperspectral Imaging System

The process to obtain the unmixed reflectance-spectra data was made. The samples were placed on a linear translation platform controlled by a stepper motor and illuminated with four lamps. The images were obtained using a Pika-NIR 320 camera that allows obtaining hyperspectral images by linear scan in the range of 900 to 1700 nm with 168 bands and 320 pixels over the cross-sectional field of view (FOV). The data were stored on a computer using SpectrononPro software.

### C. Image Processing

Of the 168 recorded bands, the first 45 were cut as they did not provide significant spectral information, finally obtaining 123 working bands. This was applied to the two studied systems. The virtual dimensionality of each image was

This work was supported in part by CONCYTEC under Grants N. 168 and N.169.

H. A. and L. Ch. are with Facultad de Ciencias, Universidad Nacional de Ingeniería, Lima, Perú (e-mail: hebbert.apaza.m@uni.pe, lcheveza@uni.pe).

H. L. Author is with Facultad de Ciencias, Universidad Nacional de Ingeniería, Lima, Perú (corresponding author, phone: 051-996706444; fax: 051 4810824; e-mail: hloro@uni.edu.pe).

estimated using the second moment linear dimensionality (SML) method [9]. Next, the minimal noise fraction (MNF) transform [10] was used to reduce dimensionality. The noise covariance matrix was estimated using the residual analysis method taking advantage of the intraband correlation [11]. Then the endmembers of each image were extracted using the simplex growing algorithm (SGA) [12]. Once the endmembers were identified, the normalization process proposed in [13] was applied over the hyperspectral data as well as over references data used, in order to reduce spectral variability and environmental and texture effects present in the recorded data. The obtained final spectra were compared and the materials present in each image were identified.

Finally, four hyperspectral unmixing techniques were applied: LSU [14], non-negatively constrained least squares unmixing (NCLSU) [15], FCLSU [16] and scaled constrained least squares unmixing (SCLSU) [17]. To evaluate the performance of each method rRMSE is used from the point of view of data reconstruction [18]. All data analysis was performed using R software version 4.0.2.

## III. Results and Discussion

### A. HSI with Plastic

After the application of the SML technique a 15 dimension was found in image 1, with a significance level of $6.25 \times 10^{-4}$. In other words, the endmembers that we had to look for are 16 (one more than the dimension of the subspace). To find them, the MNF transformation was used where the first 15 images were retained, after applying this transformation. The SG algorithm was applied to these 15 images to find the 16 endmembers present in image 1. Fig. 1 shows the location within the image of the extracted endmembers.

Fig. 1 Localization of endmembers in image 1. Endmembers were found using SG algorithm. This image contains plastic 1 and almond seeds, with a background

Fig. 2 shows the spectra of the endmembers extracted after the application of the SG algorithm. The identification of the spectra is carried out using reference spectra of each element previously measured. From Fig. 2 it is easy to visualize the variability existing between the same class of materials, for example in the case of almond seeds differences in scale are observed, such as the predominant variability in the hyperspectral data, so we normalize each spectrum contained in each pixel as well as the reference spectra to decrease variability. Next, the 4 spectral unmixing methods were applied. Table I shows the results obtained by each spectral unmixing method, where it can be clearly seen that the LSU method shows bad results since it estimates - 0.3% abundance of plastic 1 which does not agree with the abundance that must be greater than or equal to zero. Continuing with the analysis of the results obtained from Table I, it is observed that the NCLSU, FCLSU and SCLSU methods show similar results, this is due to the fact that they use restrictions on percentages of abundance, such as that they should not take negative values unlike of the LSU method that does not use constraints.

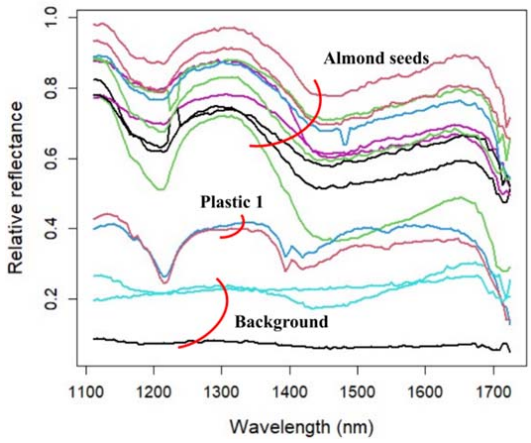


Fig. 2 Spectra of the extracted endmembers. After comparison with spectra references, we identify them with almond, plastic and background

TABLE I
Percentages of Abundance Obtained by each Method (%)

| Method | Almond | Plastic 1 | Background |
|---|---|---|---|
| LSU | 62.094 | -0.301 | 38.207 |
| NCLSU | 54.130 | 4.098 | 41.810 |
| FCLSU | 54.073 | 4.105 | 41.822 |
| SCLSU | 54.082 | 4.093 | 41.826 |

We also carried out an evaluation of the performance in the identification of an element present in the image using the 4 unmixing methods. Results are presented using a pixel color map where a 1 color value determines a total presence of the element and a 0 color value, a total absence of the element. Fig. 3 shows the resulting color maps after the application of the 4 spectral unmixing methods. As can be seen in this figure, the LSU method shows a low performance in the identification of the almond, plastic 1 and background of image 1, with some negative values in the identification scale for plastic 1 (also showed in Table I) which are not consistent with the expected results. Likewise, in Fig. 3 it is observed that the identification maps of the NCLSU, FCLSU, SCSLU methods are similar and also the identification scales that accompany each image shows values greater than or equal to zero. FCLSU and SCSLU methods give identification values lower than or equal to 1 since these last two methods implement this restriction. It can also be observed that the NCLSU method

has identification values slightly higher than 1 which are not consistent. Although there is still a low performance for a more precise classification of almond seeds and background, plastic managed to be identified by all four methods as shown in Fig. 3.

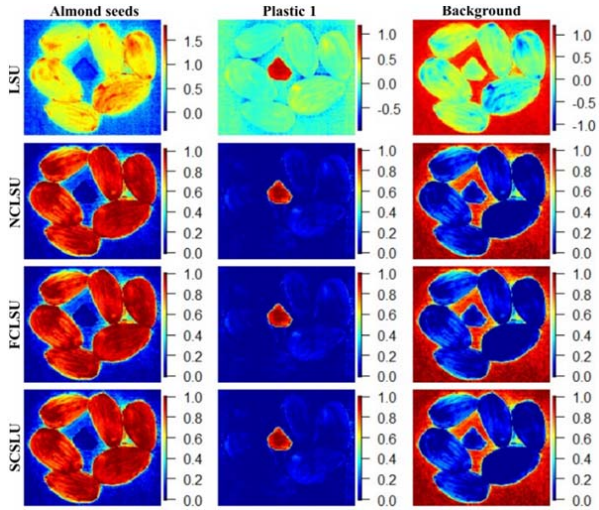


Fig. 3 Identification maps for detection of plastic, almond and background in image 1

### *B. HSI with Microplastic*

The analysis described in Subsection *A* for HSI with plastic was also applied to the second hyperspectral image, image 2, which contains a mixture of microplastic and almond flour. The SML dimensionality estimated a dimensionality of 27 for this image with a significance level of $6.25 \times 10^{-4}$. Fig. 4 shows the location of the 28 endmembers found using the SGA method on the transformed image using MNF.

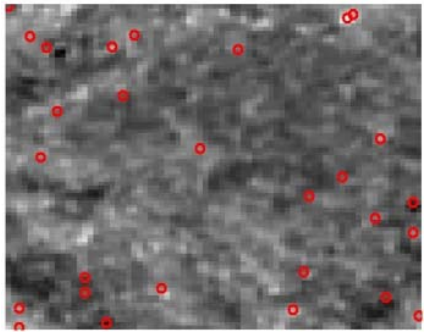

Fig. 4 Localization of endmembers in image 2. Endmembers were found using SG algorithm. This image contains almond flour and microplastic

Figs. 5 and 6 show the normalized reference spectra and hyperspectral data of the normalized endmembers obtained by SG algorithm respectively.

From Fig. 5 we can see that almond flour spectrum (black line) has pronounced absorption peaks at 1209 and 1709 nm, and for microplastic there are absorption peaks at 1145, 1209, 1647 and 1683 nm. Fig. 6 shows that the obtained endmembers present absorption peaks at 1145 nm and 1683 nm, which do not correspond to almond flour, showing that there is a foreign material within it. This material corresponds to microplastic. In order to quantify the amount of microplastic contained in this image, the 4 spectral unmixing techniques described above were applied and the obtained results are shown in Table II. It can be seen that the four methods do not give the real values, although we can consider that the values obtained are quite close, with a relative error of 4.6% for almonds and 2.2% for plastic. Likewise, identification maps were prepared to visualize the presence of microplastic in almond flour. As in the case of the image with plastic, results show that the LSU technique is the one that shows a lower performance, giving even negative values, while the other three show similar results with a performance superior to LSU.

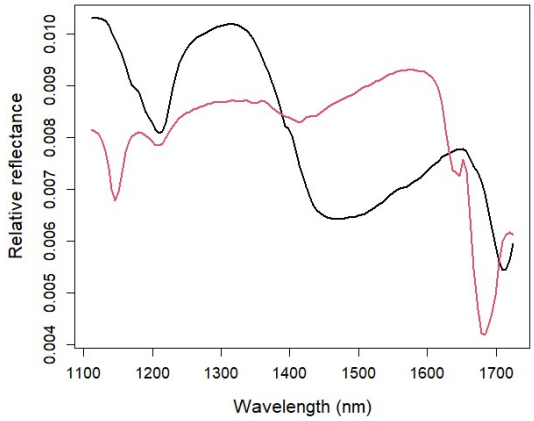


Fig. 5 Normalized reference spectra. In black, almond flour and in red, microplastic

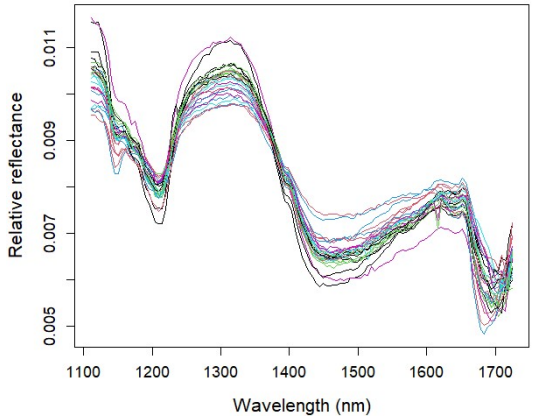


Fig. 6 Normalized endmembers spectra found using SGA

Table III shows the estimated rRMSE for each method. It can be seen that the 4 methods show very similar values. NCLSU, FCLSU and SCLSU rRMSE values are lower than that corresponding to the LSU method.

TABLE II
PERCENTAGES OF ABUNDANCE OBTAINED BY EACH METHOD (%)

| Method | Almond flour (83,33%) | Microplastic (16,66%) |
|---|---|---|
| LSU | 87.17 | 12.93 |
| NCLSU | 87.07 | 13.03 |
| FCLSU | 87.02 | 12.97 |
| SCLSU | 86.97 | 13.03 |

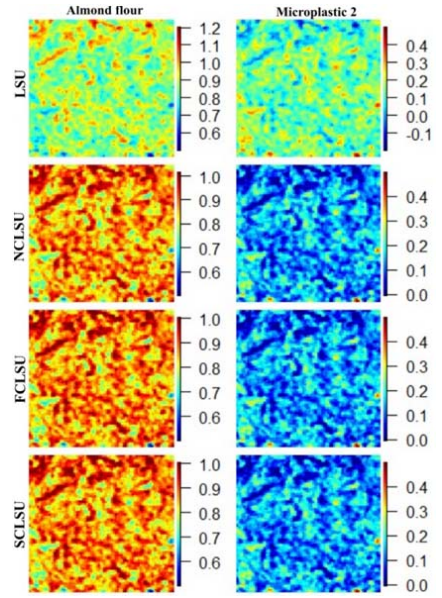


Fig. 7 Identification maps for detection of almond flour and microplastic in image 2

TABLE III
QUANTITATIVE PERFORMANCE OF EACH METHOD FOR MICROPLASTIC

| Method | rRMSE |
|---|---|
| LSU ($10^{-2}$) | 3.67 |
| NCLSU ($10^{-2}$) | 3.57 |
| FCLSU ($10^{-2}$) | 3.58 |
| SCLSU ($10^{-2}$) | 3.53 |

## IV. CONCLUSIONS

In this work, 4 hyperspectral unmixing techniques are evaluated for their application in the detection and quantification of plastic with almond seeds and of microplastic mixed with almond flour. According to the obtained results, the NCLSU, FCLSU, SCLSU methods show better results compared to LSU. These techniques manage to find the region where the plastic is found and also manage to quantify the amount of microplastic contained in the almond flour, finding 13.03% abundance of microplastics and 86.97% of almond flour estimated by the SCLSU method compared to 16.66% of microplastics and 83.33% abundance of almond flour prepared for the experiment. This work also shows the feasibility of applying near-infrared HSI for the detection of plastic contaminants in food. Additional studies are needed to improve the precision in the detection and quantification of microplastics in food.

## ACKNOWLEDGMENT

A. A. and L. Ch. wish to thank to FONDECYT-UNI Fellowship Postgraduate Program.

## REFERENCES

[1] Bouwmeester, H., Hollman, P. C., & Peters, R. J. "Potential health impact of environmentally released micro-and nanoplastics in the human food production chain: experiences from nanotoxicology". *Environmental science & technology*, *49*(15), 2015, pp. 8932-8947.
[2] Farrell, P., & Nelson, K., "Trophic level transfer of microplastic: *Mytilus edulis* (L.) to *Carcinus maenas* (L.)". *Environmental pollution*, *177*, 2013, pp.1-3.
[3] Shan, J., Zhao, J., Zhang, Y., Liu, L., Wu, F., & Wang, X. "Simple and rapid detection of microplastics in seawater using hyperspectral imaging technology". *Analytica Chimica Acta*, *1050*, 2019, 161-168.
[4] Kwon, J. H., Chang, S., Hong, S. H., & Shim, W. J., Microplastics as a vector of hydrophobic contaminants: Importance of hydrophobic additives. *Integrated Environmental Assessment and Management*, *13*(3), 2017, pp. 494-499.
[5] Wright, S. L., Thompson, R. C., & Galloway, T. S., "The physical impacts of microplastics on marine organisms: a review". *Environmental pollution*, *178*, 2013, pp. 483-492.
[6] Law, K. L., & Thompson, R. C. (2014). Microplastics in the seas. *Science*, *345*(6193), 2014, pp. 144-145.
[7] Sun, D. W. (Ed.), "*Hyperspectral imaging for food quality analysis and control*". Elsevier, 2010.
[8] Sun, D. W. (Ed.), "*Infrared spectroscopy for food quality analysis and control*". Academic press, 2009.
[9] Bajorski, P. "Second moment linear dimensionality as an alternative to virtual dimensionality". *IEEE transactions on geoscience and remote sensing*, *49*(2), 2010, pp. 672-678.
[10] Green, A. A., Berman, M., Switzer, P., & Craig, M. D. "A transformation for ordering multispectral data in terms of image quality with implications for noise removal". *IEEE Transactions on geoscience and remote sensing*, *26*(1), 1988, pp. 65-74.
[11] Chang, C. I., & Du, Q. "Estimation of number of spectrally distinct signal sources in hyperspectral imagery". *IEEE Transactions on geoscience and remote sensing*, *42*(3), 2004, pp. 608-619.
[12] Chang, C. I., Wu, C. C., Liu, W., & Ouyang, Y. C., "A new growing method for simplex-based endmember extraction algorithm". *IEEE transactions on geoscience and remote sensing*, *44*(10), 2006, 2804-2819.
[13] Polder, G., Van der Heijden, G. W. A. M., & Young, I. T., "Hyperspectral image analysis for measuring ripeness of tomatoes", 2000.
[14] Van der Meer, F., & De Jong, S. M., "Improving the results of spectral unmixing of Landsat Thematic Mapper imagery by enhancing the orthogonality of end-members". *International Journal of Remote Sensing*, *21*(15), 2000, pp. 2781-2797.
[15] Chang, C. I., & Heinz, D. C., "Constrained subpixel target detection for remotely sensed imagery". *IEEE transactions on geoscience and remote sensing*, *38*(3), 2000, pp. 1144-1159.
[16] Heinz, D. C., "Fully constrained least squares linear spectral mixture analysis method for material quantification in hyperspectral imagery". IEEE transactions on geoscience and remote sensing, 39(3), 2001, pp. 529-545.
[17] Veganzones, M. A., Drumetz, L., Tochon, G., Dalla Mura, M., Plaza, A., Bioucas-Dias, J., & Chanussot, J. "A new extended linear mixing model to address spectral variability". In 2014 6th Workshop on Hyperspectral Image and Signal Processing: Evolution in Remote Sensing (WHISPERS), IEEE, 2014, pp. 1-4.
[18] Hong, D., Yokoya, N., Chanussot, J., & Zhu, X. X., "An augmented linear mixing model to address spectral variability for hyperspectral unmixing". IEEE Transactions on Image Processing, 28(4), 2018, pp. 1923-1938.